HHS Public Access

Author manuscript

Exp Eye Res. Author manuscript; available in PMC 2016 November 01.

Published in final edited form as:

Exp Eye Res. 2015 November ; 140: 149–158. doi:10.1016/j.exer.2015.08.026.

Structure of Zebrafish IRBP Reveals Fatty Acid Binding

Debashis Ghosh[1,*,†], **Karen M. Haswell**[1], **Molly Sprada**[2,*], and **Federico Gonzalez-Fernandez**[2,†,3,4,**]

[1]Department of Pharmacology, SUNY Upstate Medical University, Syracuse, New York

[2]Medical Research Service of G.V. (Sonny) Veterans Affairs Medical Center, Jackson, Mississippi

[3]Departments of Ophthalmology and Pathology, UMMC, Jackson, Mississippi

[4]SUNY Eye Institute, State University of New York

Abstract

Interphotoreceptor retinoid-binding protein (IRBP) has a remarkable role in targeting and protecting all-*trans* and 11-*cis* retinol, and 11-*cis* retinal during the rod and cone visual cycles. Little is known about how the correct retinoid is efficiently delivered and removed from the correct cell at the required time. It has been proposed that different fatty composition at that the outer-segments and retinal-pigmented epithelium could have an important role is regulating the delivery and uptake of the visual cycle retinoids at the cell-interphotoreceptor-matrix interface. Although this suggests intriguing mechanisms for the role of local fatty acids in visual-cycle retinoid trafficking, nothing is known about the structural basis of IRBP-fatty acid interactions. Such regulation may be mediated through IRBP's unusual repeating homologous modules, each containing about 300 amino acids. We have been investigating structure-function relationships of Zebrafish IRBP (zIRBP), which has only two tandem modules (z1 and z2), as a model for the more complex four-module mammalian IRBP's. Here we report the first X-ray crystal structure of a teleost IRBP, and the only structure with a bound ligand. The X-ray structure of z1, determined at 1.90Å resolution, reveals a two-domain organization of the module (domains A and B). A deep hydrophobic pocket was identified within the N-terminal domain A. In fluorescence titrations assays, oleic acid displaced all-*trans* retinol from zIRBP. Our study, which provides the first structure of an IRBP with bound ligand, supports a potential role for fatty acids in regulating retinoid binding.

[†]Corresponding Authors: Debashis Ghosh, Department of Pharmacology. SUNY Upstate Medical University, Room 6310, Weiskotten Hall, 750 East Adams St., Syracuse, NY 13210, ghoshd@upstate.edu, Telephone: (315) 464-9677, Fax: (315) 464-8014. Federico Gonzalez-Fernandez, Medical Research Service, G.V. (Sonny) Montgomery Veterans Affairs Medical Center, 1500 East Woodrow Wilson Drive, Jackson, Mississippi 39216, Federico.Gonzalez-Fernandez@VA.gov, Telephone: (716)-863-2291, Fax: 601-364-1390.
[*]This work was initiated when these authors were at the Hauptman-Woodward Institute, Buffalo, NY 14203
[**]This work was initiated when this author was at the Buffalo VAMC, and Department of Ophthalmology, SUNY, Buffalo, New York 14215

Accession code

Coordinates and data are deposited with the Protein Data Bank under accession code 4LUR.

Keywords

Interphotoreceptor retinoid-binding protein; Interphotoreceptor matrix; Retina; Visual cycle; Zebrafish; Oleic acid; X-ray structure

1. Introduction

During rod and cone visual cycles, 11-*cis* retinal bound to rhodopsin is isomerized to all-*trans* retinal by absorbed photon energy (Lamb and Pugh, 2006; McBee et al., 2001). All-*trans* retinal is then released from rhodopsin, reduced by retinol dehydrogenase, and transported to the retinal-pigmented epithelium (RPE), or Müller cells to be enzymatically re-isomerized (Lamb and Pugh, 2004; Marmor and Martin, 1978; Thompson and Gal, 2003). The rods receive 11-*cis* retinal from the RPE, whereas 11-*cis* retinol is released to the cones by Müller glia. Cones, unlike rods, can oxidize 11-*cis* retinol to 11-*cis* retinal (Mata et al., 2002; Mata et al., 2005; Muniz et al., 2007; Trevino et al., 2005; Wolf, 2004) to complete the cycle. Both cycles require the efficient exchange of 11-*cis* retinal, 11-*cis* retinol, and all-*trans* retinol between the photoreceptors, RPE, and Müller cells, which are separated by a unique extracellular material known as the interphotoreceptor matrix (IPM). The mechanism(s) allowing the efficient targeting of specific retinoids for release or uptake at the correct cell at the correct time are important largely unknown questions.

Interphotoreceptor retinoid-binding protein (IRBP), which is essential to the integrity of the retina (Arno et al., 2015), is thought to play a role in protecting, and efficiently targeting and translocating retinoids between the cells bordering the IPM. One possibility, is that the pericellular environment regulates the binding of IRBP to the cell surface and/or its affinity for specific retinoids (Wolf, 1998). Such interactions would result in conformation changes in IRBP promoting the release, or uptake of specific retinoids at the cell surface. As the major soluble protein component of the IPM, IRBP has been proposed to play several roles in the visual cycle (Gonzalez-Fernandez, 2003, 2012; Gonzalez-Fernandez and Ghosh, 2008; Lamb and Pugh, 2004, 2006; Liou et al., 1991; McBee et al., 2001; Nickerson et al., 1991; Pepperberg et al., 1993). IRBP facilitates the release of all-*trans* retinol from bleached rods (Qtaishat et al., 2005; Tsina et al., 2004a; Wu et al., 2007), and 11-*cis* retinal from the RPE (Carlson and Bok, 1992, 1999; Edwards and Adler, 2000; Flannery et al., 1990). IRBP was recently shown to facilitate the uptake of all-*trans* retinol and release of 11-*cis* retinol from Müller cells *in vitro* (Betts-Obregon et al., 2014). Furthermore, IRBP effectively delivers all-*trans* retinol and 11-*cis* retinal to the RPE (Flannery et al., 1990; Jin et al., 2009; Okajima et al., 1989), and rod and cone outer segments (Duffy et al., 1993; Jin et al., 2009; Okajima et al., 1990; Parker et al., 2011). Finally, an important emerging function of IRBP is protect visual-cycle retinoids from photodecomposition within the interphotoreceptor matrix (Crouch et al., 1992; Gonzalez-Fernandez et al., 2015; Gonzalez-Fernandez et al., 2014).

zIRBP may have important functions in the adult and developing zebrafish retina. In the adult, zIRBP turnover and mRNA expression is regulated by circadian and light-driven mechanisms that act differentially on the various photoreceptor subtypes (Cunningham and Gonzalez-Fernandez, 2000; Rajendran et al., 1996). The temporal and spatial patterns of

IRBP expression by the RPE and retina are consistent with a role in retinal development and suggest coordination of RPE and photoreceptor differentiation (Stenkamp et al., 1998). Morpholino knock down of transcription factors controlling sets of retinal specific genes can disrupt retinal development and photoreceptor differentiation (Li et al., 2010; Li et al., 2015). However, the specific contribution of decreased zIRBP expression to these phenotypes cannot be determined as multiple photoreceptor genes are affected simultaneously. Nevertheless, the findings are consistent with a variety of studies suggesting that IRBP has a role in retinal development and maintenance (DesJardin et al., 1993; Gonzalez-Fernandez and Healy, 1990; Gonzalez-Fernandez et al., 1993; Hauswirth et al., 1992; Hessler et al., 1996; Wisard et al., 2011).

Its multi-module structure, unique among the retinoid-binding proteins, may underlie IRBP's function in the visual cycle. From the agnatha to tetrapod species, IRBP is composed of four homologous modules, designated by the numbers one through four. Each module contains roughly 300 amino acid residues distributed into two domains, A and B (Dettai and Lecointre, 2008). The individual modules appear to represent functional units of the protein (Baer et al., 1998a; Gonzalez-Fernandez et al., 1998; Gonzalez-Fernandez et al., 2007; Gross et al., 2000; Loew et al., 2001; Nickerson et al., 1998). X-ray crystallographic and site-directed mutagenesis studies of *Xenopus* apo IRBP-module 2 (x2) have identified a novel hydrophobic cavity within domain A (Gonzalez-Fernandez et al., 2009), and a hydrophobic cleft in domain B. Although this cleft was thought to represent the key ligand-binding site, *in silico* ligand-docking studies and site directed mutagenesis experiments indicated that the hydrophobic cavity within domain A is the major ligand-binding site (Gonzalez-Fernandez et al., 2009). Each of the modules appears to contain similar, but not identical cavities, suggesting the existence of binding sites tailored for different ligands and/or functions (Gonzalez-Fernandez et al., 2007). Such ligands could include all-*trans* retinol, 11-cis *retinol* and retinal, and vitamin A1/A2 (Allison et al., 2004).

Its ability to bind physiologically relevant fatty acids suggests new functions for IRBP and/or mechanisms to regulate retinoid delivery and uptake. IRBP readily binds a variety of fatty acids *in vitro* (Baer et al., 1998b; Lin et al., 1997; Putilina et al., 1993; Semenova and Converse, 2003). Furthermore, native bovine IRBP contains covalently and noncovalently bound fatty acids (Bazan et al., 1985). It has been speculated that IRBP has a role in the translocation of fatty acids particularly 22:6n-3 between the RPE and retina (Bazan et al., 1992). Another function of fatty acid binding may be to regulate the relative affinities of all-*trans* retinol and 11-*cis* retinal for IRBP during the visual cycle. This idea was prompted by the observation that 22:6n-3 but not palmitic acid results in the specific release of 11-*cis* retinal from the stronger of IRBP's two retinol-binding sites (Chen et al., 1996; Chen et al., 1993). Given the steep 22:6n-3 concentration gradient between photoreceptors and RPE, the local fatty acid environment could play an important role in regulating the cell specific uptake and release of visual cycle retinoids [reviewed in (Wolf, 1998)].

If we are to ever understand the role of fatty acids in the regulation of IRBP's function, IRBP's fatty acid-binding site(s) will have to be located and structurally characterized. That fatty acids could bind the hydrophobic cleft in domain B was predicted from comparisons of the structure of an individual apo-IRBP module and the solved photosystem II D1 C-

terminal-processing protease structure (Loew and Gonzalez-Fernandez, 2002a). However, the complexity of IRBP's 4-module structure has challenged research in this area. As a result, no structural data of the holo-IRBP is available. We initiated our structural studies with oleic acid given its known tight binding to bovine IRBP (Semenova and Converse, 2003).

Zebrafish provides a powerful system to uncover the relationships between IRBP's module structure and its function. In contrast to the 4-module structure of IRBP in other vertebrates, the number of modules of zebrafish IRBP (zIRBP) genes is limited to two or three. Zebrafish *IRBP gene I*, which is expressed by cell(s) in the inner nuclear layer, is composed of modules homologous to 1+2+3 in other vertebrates; *IRBP gene II* is expressed by the photoreceptors and RPE, and corresponds to IRBP modules 1+4 (Nickerson et al., 2006; Rajendran et al., 1996; Stenkamp et al., 1998). Zebrafish, which possesses both rod and cone visual cycles, may therefore provide a unique opportunity to uncover the relationship between the IRBP's module structure, and function (Collery et al., 2008; Fleisch and Neuhauss, 2010; Fleisch et al., 2008; Schonthaler et al., 2007; Takahashi et al., 2011; Wang and Kefalov, 2011).

2. Materials and Methods

2.1. Expression and purification

The full-length zIRBP (*IRBP gene II*, the product of which is two tandem homologous modules of about 300 amino acids each) was originally obtained by screening a cDNA library as previously described (Rajendran et al., 1996). The full-length zIRBP cDNA was subcloned via ligation independent cloning with the addition of the TEV protease recognition site immediately downstream (3') to factor Xa recognition site and immediately upstream (5') of the zIRBP gene in the pET-30 Xa/LIC vector, and an expression clone was prepared in *Escherichia coli* BL21(DE3) cells (Haun et al., 1992). Cultures were grown at 37°C in Luria Broth (LB) containing 30μg/mL Kanamycin and were induced with 1 mM IPTG at a cell density (OD_{600}) of 0.6–0.8. Proteins were expressed for 22–24 hours at 19°C.

Selenomethionine (Se-Met)-substituted zIRBP was produced by overexpressing the TEV-zIRBP construct in *E. coli* strain B834(DE3)pLysS, a methionine auxotroph (Owens et al., 2007). Cultures were grown at 37°C in SelenoMethionine medium (Molecular Dimensions) containing 40mg/L selenomethionine and 30μg/mL Kanamycin. The temperature was reduced to 19°C when the cultures reached a cell density (OD_{600}) of ~0.6, and expression was induced with 1 mM IPTG. The cultures continued to grow an additional 20–24 hours.

Both zIRBP and Se-Met-zIRBP were purified using the following method. Cells were harvested by centrifugation (6260*g* for 20 min at 4°C), and pellets were stored at −80°C for at least 24 hours. Cell pellets were resuspended in buffer A (50 mM Tris-HCl pH 7.5 at 4°C, 50 mM NaCl, 1 mM dithiothreitol) with 1mg/mL lysozyme, approximately 5μg/mL DNase, and broad-spectrum protease inhibitors (Sigma), and then microfluidized (Microfluidics). Cell debris was removed by centrifugation (96,000*g* for 15 min at 4°C). All purification columns were run on Äkta FPLC (GE Healthcare) at 4°C and pre-equilibrated with buffer A. Cell lysate was applied to a 5 mL HisTrap HP column (GE Healthcare). The protein was

eluted using a linear imidazole gradient (0–300 mM imidazole in buffer A). TEV protease was then added to the pooled fractions in a ratio of 3 mg TEV protease to 8mg zIRBP and dialyzed overnight in buffer A at 4°C to reduce the imidazole concentration to less than 1.5 mM. Cleaved zIRBP was then located in the unbound fractions of a second 5mL HisTrap HP column. The cleaved zIRBP was then applied to a charged anion exchange column (HiTrap Q HP, GE Healthcare) and eluted in a linear gradient of buffer A containing 1M NaCl. Fractions containing zIRBP were pooled and the NaCl concentration was adjusted to 100 mM. The purity of zIRBP was judged to be >98% by SDS-PAGE. Using centrifugal ultrafiltration, the protein was concentrated to 15 mg/mL as determined by SDS-PAGE and OD_{280}. Ten mM retinol and 3 M oleic acid stocks were dissolved in Argon overlaid PEG 200 and ethanol, respectively. All-*trans* retinol was added to a concentration of 55 μM, and oleic acid was added to a concentration of 43 μM. The protein was allowed to incubate in the presence of ligand for 90 min. before the solution was filtered (0.2 μm) to remove particulate matter prior to crystallization.

2.2. Crystallization and X-ray diffraction

The recombinant zIRBP was crystallized by the sitting-drop vapor diffusion method in 24 well plates at 23°C. Protein solutions at a concentration of 15 mg/mL were mixed with the reservoir solutions of 35–44% polyethylene glycol 8000 in 100 mM HEPES pH 7.5 buffer containing 100 mM NaBr in the 1:1, 2:1, 2.5:1, and 3:1 drop to volume ratios (DVR), in total drop volumes ranging from 2–16 μL, and vapor diffused against the reservoir solutions. The best DVR was 2:1. While we obtained more crystals at this DVR, the crystals grew over the entire range. The crystallization conditions for IRBP from other species are similar, but not the same. Polyethylene glycol is one of the most frequently used protein crystallization agents; many protein families have been crystallized with polyethylene glycol 2000–8000 at or about the neutral pH. Plate-shaped crystals appeared in about a week and continued to grow for a few more weeks. The crystals were cryocooled by the addition of 10% glycerol as the cryoprotectant and plunging them into liquid nitrogen. They were maintained at the liquid nitrogen temperature during diffraction data collection. Tens of crystals were screened to select one for the data collection. We gathered complete data sets on at least 4 crystals from different purification batches (experiments), always with the same results i.e. zIRBP cleaved and z1 crystallized. The space group is $P2_12_12$ and the unit cell parameters are a=88.30Å, b=97.77Å, c=41.21Å, α=β=γ=90°, suggesting that there is only one of the two modules in the asymmetric unit. The Se-Met derivative zIRBP crystals were also prepared in a similar way.

Diffraction data on the native and Se-Met derivative crystals of zIRBP were collected at the synchrotron X-ray beamline 19ID, the Structural Biology Center, Advanced Photon Source, Argonne National Laboratory, Argonne, IL. Three data sets from two crystals were gathered with the X-ray photon energy tuned at peak, inflection and remote points of the selenium absorption edge. Data sets at the peak and a remote higher energy point were collected to 1.90Å resolution and at the inflection point to 2.30Å. Data collection and processing statistics are shown in Table 1A.

2.3. Determination of the structure of zIRBP

Phasing by multiple anomalous dispersion (MAD) alone was insufficient to yield an interpretable electron density map. The structure was determined by a combination of MAD and molecular replacement methods. CCP4 package of software (Winn et al., 2011) was used for the purpose. Rotation and translation function searches using Molrep - auto MR routine with the C-terminal B domain (all atoms) of 1J7X were successful in correctly positioning the molecule. Phase combined and anomalous difference maps were used to build the complete model. The final model showed anomalous difference density in 9 Se positions out of 11 possible Se-Met side chains. The refinement was carried out by Refmac5 (Murshudov et al., 1997) in CCP4. The initial model was refined at 1.90 Å using the best data sets collected at the peak and remote wavelengths. The omit map calculated with the data at the peak wavelength showed slightly better electron density for oleic acid. The final R-factor for all reflections is 0.219 and the R-free value is 0.268. While elucidating the structure, we discovered that the two-module containing zIRBP polypeptide was proteolytically cleaved between the modules during the crystallization process, and only module 1 (309 amino acids of a total 594) crystallized. Most of the residues had well-defined electron densities for the side chains, which conformed to the known sequence. The final model included 309 amino acids, one oleic acid, three glycerol molecules, one HEPES and 166 water molecules. Because of the ambiguous nature of the electron density, no ligand could be modeled in the domain B cavity. Table 1B summarizes the parameters from the refinement. Coordinates and data are deposited in the Protein Data Bank under the accession code 4LUR.

2.4. Ligand-binding studies

The binding of all-*trans* retinol to zIRBP and competition by oleic acid was analyzed by fluorescence spectroscopy. All-*trans* retinol at a purity of 99% by HPLC was obtained from Fluka (Buchs). Working stocks were prepared fresh in ethanol and held under argon at −80°C. The extinction coefficient of all-*trans* retinol in ethanol was taken as 38,300 $M^{-1}cm^{-1}$, 325 nM (Szuts and Harosi, 1991). The binding of all-*trans* retinol to zIRBP was characterized in titrations using a DM 45 scanning spectrofluorimeter (OnLine Instrument Systems, Inc., Bogart, GA) (Ward, 1985). Titrations monitoring enhancement of retinol fluorescence were carried out as previously described (Gonzalez-Fernandez et al., 2007; Gonzalez-Fernandez et al., 2009). Titrations were performed by adding 0.5 μL aliquots of all-*trans* retinol in ethanol directly into the cuvette containing a 1μM solution of recombinant protein or buffer. The solution was thoroughly mixed by inversion and all-*trans* retinol aliquots were added at 1 min intervals. The final alcohol concentration never exceeded 2%. Enhancement of retinol fluorescence was followed by monitoring the increase in retinol fluorescence in the presence of protein compared to buffer alone (all-*trans* retinol: excitation, 330 nm; emission, 480 nm). The titration of all-*trans* retinol fluorescence enhancement was performed in the absence of and at increasing concentrations of oleic acid between 0.0 and 0.112 μM. The all-*trans* retinol binding data at each oleic acid concentration was fitted by non-linear least squares to a curve using two different models. First, the experimental data was analyzed by GraphPad Prism Version 6 (GraphPad Software, La Jolla, CA, www.graphpad.com) using the “one site- specific binding with Hill

slope" model. The analysis generated a K_d value (ligand concentration that binds to half the receptor sites at equilibrium) and a Hill coefficient *n* at each all-*trans* retinol concentration. Next, the titration data was analyzed by Origin 8.5 (OriginLab, Northhampton, MA) using the Hill function model to yield a Michaelis constant K and *n*, the number of cooperative binding sites for each all-*trans* retinol concentration. Both models produced the same plots and the values for K and *n*.

2.5. Sequence alignment and homology modeling

The sequence alignment of x2, z1 and z2 was performed using the Probabilistic Consistency-based Multiple Alignment of Amino Acid Sequences (ProbCons) (Do et al., 2005). The sequence and crystal structure of the z1 was used as a template for the 3D structural alignment of the z2. The MOE-Align and MOE-Homology platforms in the Molecular Operating Environment ® 2012 software (Chemical Computing Group, Montreal, Canada) were used for this purpose. MOE-Align generated a sequence alignment of z2 to the structure of z1 emphasizing the secondary structure similarity. MOE-Homology was used in generating the 3D structures of z2 from the z1 template. This method of alignment is based on a combination of the *segment-matching* procedure of Levitt (Levitt, 1992) and an approach to the modeling of *indels* based on that of Fechteler et al (Fechteler et al., 1995). MOE-Homology created 10 models, each of which was generated by making a series of Boltzmann-weighted choices of rotamers of side chains and loop conformations from a set of protein fragments selected from the built-in library of high-resolution protein structures. The selected model was an energy-minimized average model.

3. Results

Gathering of X-ray diffraction data and analysis on many crystals from many different crystallization drops and purification experiments have firmly established that only the polypeptide containing the first 309 residues crystallizes. This polypeptide contains 300 amino acids of module 1 (z1) and 9 of module 2 (z2) (per sequence homology of the modules, Fig. 1). (We have used "module 1" or "z1" to denote synonymously, either the true repeating module sequence of the N-terminal 300 residues, or the crystallized cleavage product of 309 residues). The presence beyond T309 of a few additional residues with high thermal motion and no discernable electron density cannot be ruled out. Nevertheless, no crystal of either the full length or the cleaved second module has yet been identified.

3.1. The two-domain crystal structure of zIRBP module 1 (z1)

A ribbon representation of the X-ray crystal structure of zIRBP module 1 is shown in Fig. 2 with the N- and C-termini in blue and red, respectively. The N-terminal A domain is made of three α-helices α1, α2, and α3, and a three-stranded β-sheet that defines the inter-domain interface. One strand of the sheet (β0) is from the N-terminal segment; the other two, β8 and β9, are from the C-terminal half. The B domain comprises of five α-helices, α4 through α8, packed around a central mixed five-stranded β-sheet with strands β1, β2, β3, β6, and β7. A second β-sheet, having strands β4, β5 and the C-terminal end of β9, makes up the interfacial wall that demarcates the two domains. A dynamically mobile, extended and open polypeptide segment (between P71 and P85) ending in α4 acts as a tether between the A and

B domains. This segment in the structure of x2 was found to be disordered (Loew and Gonzalez-Fernandez, 2002a), unlike the weak but well-defined electron density for this region of z1. Fig. 3 is a superposition of z1 with the structure of x2, showing change in the relative orientation of the domains A and B between the two structures (the sequences of x2, z1 and z2 are aligned in Fig. 1). As discernable from the superposition, domain B's structures are largely unchanged. However, domain A's are rotated roughly 21 ± 4º from each other about the viewing axis at the domain interface in Fig. 3.

3.2. The oleic acid binding sites

The oleic acid binding site in domain A is shown in Fig. 2 with the refined ligand coordinates. Although a deep hydrophobic cavity in domain B in x2 was previously identified and postulated to be the retinol-binding site (Gonzalez-Fernandez et al., 2007; Gonzalez-Fernandez et al., 2009; Loew and Gonzalez-Fernandez, 2002a), structural evidence to that effect has yet to be published. Furthermore, there has been no proposal to date for a possible ligand-binding site in domain A. The X-ray data clearly show the electron density for an extended oleic acid molecule in domain A (Fig. 4). Within the cavity, delineated by the secondary structure elements α1, α2, α3, β0 and a part of β9, hydrophobic residues completely surround the oleic acid chain (Fig. 2). Atoms C5 to C18 of the bound oleic acid are embedded in a cavity formed by the residues M9, A10, and F13 from α1, M26, A29, I30, A32 and A33 from α2, V51, L52, G55, V56 and T59 from α3, V65 and V67 from β0, and V254 and V256 from β9 (Fig. 5). At the bottom of the cavity interactions of the C18-end of oleic acid with the protein atoms are relaxed (Monod et al., 1965). However, positioning of the *cis*-C9=C10- moiety at the mouth of the cavity is tight and greatly aided by the strategic location of residues A29, A32, A33 and G55, with small or no side chains (Fig. 5). The carboxylate end of oleic acid outside the cleft is likely to be more dynamically mobile and probably interacts with the polar surroundings, such as solvent molecules or even the K58 side chain poised nearby.

In domain B, a roughly spherical cavity is lined by the residues I93 and T96 from α4, V97 from β1, L109 and I111 from β2, I114, I115, A120, G124, L127, L128, I131 and W132 from α5, M141 and L143 from β3, Y158, I159, Y162 and F163 from α6, as well as some loop regions (Fig. 6). L193 from the long loop between β5 and β6 partially caps the opening to the cavity (not shown). Within the cavity, an electron density that accommodates a 9 or 10 carbon aliphatic chain in close proximity to W132 and Y162 side chains, but ambiguous beyond, has remained unexplained. Modeling suggests that the cavity is large enough to accommodate either oleic acid or all-*trans* retinol (results not shown).

3.3. Fluorometric titration of all-trans retinol binding and oleic acid competition

The result from the titration experiment is shown in Fig. 7. Table 2 summarizes the binding stoichiometry and overall K_d values. In the absence of oleic acid, the all-*trans* retinol enhancement titration suggests an average Hill coefficient (or number of cooperative binding sites *n*) of ~1.8. In the presence of oleic acid, all-trans retinol binding gradually reduced at increasing concentrations of oleic acid, The final all-*trans* retinol concentration (4μm) did not overcome the oleic acid competition. The limited solubility of all-*trans* retinol did not allow carrying out the titrations to higher ligand concentrations.

3.4. Status of the ligand binding sites in module 2 (z2) from homology modeling

The percent identity between z1 and z2 is 32.8 and the percent similarity is 54.6 based on the alignment of z1 with z2 (Fig. 1). Likewise, the percent identity between z1 and x2 is 30.1 and the percent similarity is 50.3. Because of high homology between the two modules, modeling of z2 after z1 yields a structure nearly identical to z1, except for some loops, turns and the inter-domain tether (P71 to T96), which is somewhat shorter for z2. The ligand-binding site in domain A is shown superimposed in Fig. 8. The z1 to z2 substitutions of A29 to K327, I39 to Y337, V51 to R349, and G55 to D353 create direct steric clash with the bound Oleic acid molecule in domain A and block off the entry cleft (Fig. 8). Towards the interior of the cavity, changes like I30 to L328, A33 to V331, and V56 to L354, and V254 to L547 at the bottom (not shown), result in tighter contact distances to the ligand. However, a few large hydrophobic to smaller side chain substitutions, such as M9 to A307 and F13 to I311 could open up more space for the tail end of the ligand.

Inside the B-domain cavity of z2, four smaller hydrophobic residues V97, I111, I114 and I159 in z1 are replaced by the larger F390, F404, F407, and F452, respectively (Fig. 1). Three substitutions in z2, A120 to V413, G124 to A417, and L193 to T486, narrow the opening to the cavity. Thus, homology modeling indicates that in z2 both clefts are obstructed by the substitutions of smaller amino acids by larger side chains (result not shown) and are therefore probably nonexistent. However, this observation requires validation by an experimental z2 structure.

4. Discussion

The ligand-binding pocket identified here was not predicted in previous *in silico* modeling studies of the all-*trans* retinol-binding site. Those studies called attention to a “cleft” and a “cavity” in the *Xenopus* IRBP module 2 (x2) structure. There, comparisons of the x2 structure with that of 2-enoyl-CoA hydratase complexed to octanoyl-CoA called identified to a shallow partially hydrophobic “shallow cleft” at the interface between domains A and B (Loew and Gonzalez-Fernandez, 2002a). However, subsequent mutagenesis work indicated that the retinol-binding site was more likely to be a novel hydrophobic “cavity” within domain B predicted from *in silico* docking (Gonzalez-Fernandez et al., 2007). In the present study, electron densities consistent with a bound oleic acid molecule provide the first direct evidence that a previously unrecognized deep hydrophobic pocket in domain A binds oleic acid. The average temperature of oleic acid (~68 $Å^2$) is higher than the protein environment (~45 $Å^2$), probably suggestive of higher dynamical motion or lower occupancy or both of the ligand (Rhodes, 2006). There is little doubt that B domain, the location of the putative all-*trans* retinol binding site, also has a ligand-binding cavity. However, the identity of the ligand could not be confirmed from the present results.

The architecture of the cavities in domains A and B, although similar in their hydrophobic characters, differ considerably in size and to a lesser extent, in shape. The A-domain site is smaller in volume and accommodates the fatty acid in the extended conformation. The interior of the cavity of domain B, on the other hand, is larger in volume and lined with large hydrophobic side chains and probably more rigid than the A-site. The higher overall rigidity is reflected in significantly lower average “temperature factor” of the B-domain (29.7$Å^2$) in

comparison with A (39.2Å^2). Although it appears that these sites are eliminated from module 2 due to changes in the sequence, flexibility-induced accommodation of specific ligand conformations in z2 cannot be ruled out.

The interaction of oleic acid with IRBP may be physiologically meaningful in the visual cycle. It has been proposed that regulation of retinoid affinity by fatty acids underlies cell targeting of specific retinoids during the visual cycle (Chen et al., 1996; Wolf, 1998). The local fatty-acid composition of the outer segment and RPE may have a role in directing the trafficking of retinoids in the visual cycle (Chen et al., 1996). Docosahexaneoic acid, which is abundant in the outer segments, reduces the affinity of bovine IRBP for 11-*cis* retinal, suggesting a mechanism to release this retinoid at the outer segment for visual pigment regeneration (Wolf, 1998). Future structural and biochemical studies of IRBP binding to various retinoids and fatty acid ligands will help to uncover the role of IRBP in the complex exchange of visual cycle retinoids in the rod and cone visual cycles.

The mechanism for the displacement of all-*trans* retinol by oleic acid is an interesting avenue for future research. Although it is too earlier to conclude whether the inhibition observed here represents competitive and/or non-competitive processes, our data taken together with that of others, suggests allosteric mechanism(s) should be considered. Interestingly, overlay of the structure of z1 (with bound all-*trans* retinol) with x2 (no ligand) shows a shift in the relative orientations of domains A and B (Fig. 3). Although species differences may have to be taken into account, the observation suggests that the ligand-binding domain environments in domains A and B could be interdependent. Such ligand-dependent shape changes are reminiscent of the conformation changes in bovine IRBP detected by tungsten shadowing scanning electron microscopy (Adler et al., 1987). In that study, all-*trans* retinol binding was associated with a 60 to 90° overall bending of bIRBP. Although the shift observed here for a single module was less (21 ± 4º) it should be keep in mind that bIRBP is composed of 4 modules, and therefore an additive shift within each module could account for the bend observed by electron microscopy. That the fluorescence enhancement reduction during the titration assays was not even partially rescued at high all-*trans* retinol concentrations is also consistent with noncompetitive inhibition. These considerations are in agreement with the structural determination of one ligand-binding site in each of the A and B domains, and the hypothesis that the conformational flexibility of domain A could be transmitted to the domain B site via the interfacial wall. Although more work needs to be done, our observations are consistent with a conclusion of Chen *et al*. (1986) working with bovine IRBP, “These data seem to indicate that fatty acids do not associate directly with either of the retinoid-binding pockets. Instead, the observations imply that while DHA might induce a change in the configuration of the hydrophilic site, it does not directly compete with retinoids on binding to it.” Future studies should be aimed at understanding the effect ligand binding on the structure of IRBP.

Structural studies will help us to uncover the significance of amino acid substitutions caused by hereditary retinal disease. SNP microarray homozygosity mapping identified a D1080N mutation in autosomal recessive retinitis pigmentosa (den Hollander et al., 2009). D1080, which is conserved between vertebrate and plant C-terminal-processing proteases, is required for the formation of a highly conserved salt bridge. The present study confirms that

this salt bridge is located in the scaffold of the putative all-*trans* retinol binding cavity in domain B (data not illustrated). It is, therefore, possible that disruption of the salt bridge destabilizes the ligand-binding site compromising IRBP's ability to efficiently bind, be effectively secreted (Li et al., 2013), release and/or protect retinoids from degradation. Furthermore, the appreciation of a novel hydrophobic ligand-binding cavity binding fatty acids in Domain B may be important to understanding IRBP's ability to efficiently clear retinol from bleached outer segments (Tsina et al., 2004b; Wu et al., 2007) while protecting from photodecomposition (Crouch et al., 1992; Gonzalez-Fernandez et al., 2015; Gonzalez-Fernandez et al., 2014; Parker et al., 2011). Efficient clearance of all-*trans* retinol from the outer segment could minimize bisretinoid toxic intermediates, early events in the pathogenesis of age-related macular degeneration (Sparrow et al., 2003).

Finally, it should be mentioned that the unexpected cleavage of zIRBP during crystallization despite the presence of protease inhibitors during the purification process suggests an autocatalytic function for IRBP. Although it shares no significant similarity with other retinoid-binding proteins, IRBP has homology with C-terminal transferases, and crotonases (Loew and Gonzalez-Fernandez, 2002b). The tertiary structure of x2IRBP has an overall fold similar to D1 C-terminal processing protease (D1P) without the PDZ domain (Loew and Gonzalez-Fernandez, 2002b). The IRBP fold is similar to the MEROPS database (Rawlings et al., 2012) serine peptidase classification clan SK, family S41, subfamily A (C-terminal processing peptidases, CTPases), which includes CtpA, CtpB, and CtpC peptidases and chlamydial protease-like activity factor (CPAF) (Page and Di Cera, 2008; Rawlings et al., 2012). This subfamily typically recognizes certain sequences at the carboxyl terminus of proteins, and then processes C-terminal extensions and/or makes endoproteolytic cleavages at various distances from the C-terminal recognition site. Ongoing studies in our laboratories are aimed at uncovering the functional significance of this potential autocatylic activity.

Acknowledgments

The authors wish to thank Jessica Lo and Chinaza Egbuta for performing homology and binding titration modeling. Jennifer Griswold Breen is thanked for her technical assistance during the early part of this work.

The work was supported by NIH R01 EY09412 (D.G., F.G.-F.), Merit Review Award I01BX007080 from the Biomedical Laboratory Research & Development Service of the Veterans Affairs Office of Research and Development (F.G.-F., Staff Physician), an Unrestricted Research Grant from Research to Prevent Blindness to the Department of Ophthalmology at State University of New York at Buffalo. The contents of this study do not represent the views of the Department of Veterans Affairs, or the United States Government. The Structural Biology Center at the Advanced Photon Source, Argonne, IL is operated by UChicago Argonne, LLC, for the U.S. Department of Energy, Office of Biological and Environmental Research under contract DE-AC02-06CH11357.

Abbreviations used

IRBP	Interphotoreceptor retinoid-binding protein
zIRBP	Zebrafish IRBP
xIRBP	Xenopus IRBP
OLEIC ACID	oleic acid
ATR	all-*trans* retinol

RPE	retinal-pigmented epithelium
IPM	interphotoreceptor matrix
CTPase	carboxy terminus processing protease

References

Adler AJ, Stafford WF 3rd, Slayter HS. Size and shape of bovine interphotoreceptor retinoid-binding protein by electron microscopy and hydrodynamic analysis. J Biol Chem. 1987; 262:13198–13203. [PubMed: 3654607]

Allison WT, Haimberger TJ, Hawryshyn CW, Temple SE. Visual pigment composition in zebrafish: Evidence for a rhodopsin-porphyropsin interchange system. Vis Neurosci. 2004; 21:945–952. [PubMed: 15733349]

Arno G, Hull S, Robson AG, Holder GE, Cheetham ME, Webster AR, Plagnol V, Moore AT. Lack of interphotoreceptor retinoid binding protein, caused by homozygous mutation of RBP3, is associated with high myopia and retinal dystrophy. Invest Ophthalmol Vis Sci. 2015

Baer CA, Retief JD, Van Niel E, Braiman MS, Gonzalez-Fernandez F. Soluble expression in E. coli of a functional interphotoreceptor retinoid-binding protein module fused to thioredoxin: correlation of vitamin A binding regions with conserved domains of C-terminal processing proteases. Exp Eye Res. 1998a; 66:249–262. [PubMed: 9533851]

Baer CA, Van Niel EE, Cronk JW, Kinter MT, Sherman NE, Braiman MS, Gonzalez-Fernandez F. Arginine to glutamine substitutions in the fourth module of Xenopus interphotoreceptor retinoid-binding protein. Mol Vis. 1998b; 4:30–43. [PubMed: 9873068]

Bazan NG, Gordon WC, Rodriguez de Turco EB. Docosahexaenoic acid uptake and metabolism in photoreceptors: retinal conservation by an efficient retinal pigment epithelial cell-mediated recycling process. 1992; 318:295–306.

Bazan NG, Reddy TS, Redmond TM, Wiggert B, Chader GJ. Endogenous fatty acids are covalently and noncovalently bound to interphotoreceptor retinoid-binding protein in the monkey retina. J Biol Chem. 1985; 260:13677–13680. [PubMed: 3932343]

Betts-Obregon BS, Gonzalez-Fernandez F, Tsin AT. Interphotoreceptor Retinoid-Binding Protein (IRBP) Promotes Retinol Uptake and Release by Rat Muller Cells (rMC-1) In Vitro: Implications for the Cone Visual Cycle. Invest Ophthalmol Vis Sci. 2014; 55:6265–6271. [PubMed: 25183762]

Carlson A, Bok D. Promotion of the release of 11-cis-retinal from cultured retinal pigment epithelium by interphotoreceptor retinoid-binding protein. Biochemistry. 1992; 31:9056–9062. [PubMed: 1390692]

Carlson A, Bok D. Polarity of 11-cis retinal release from cultured retinal pigment epithelium. Investigative Ophthalmology and Visual Science. 1999; 40:533–537. [PubMed: 9950616]

Chen Y, Houghton LA, Brenna JT, Noy N. Docosahexaenoic acid modulates the interactions of the interphotoreceptor retinoid-binding protein with 11-cis-retinal. J Biol Chem. 1996; 271:20507–20515. [PubMed: 8702792]

Chen Y, Saari JC, Noy N. Interactions of all-trans-retinol and long-chain fatty acids with interphotoreceptor retinoid-binding protein. Biochemistry. 1993; 32:11311–11318. [PubMed: 8218196]

Collery R, McLoughlin S, Vendrell V, Finnegan J, Crabb JW, Saari JC, Kennedy BN. Duplication and divergence of zebrafish CRALBP genes uncovers novel role for RPE- and Muller-CRALBP in cone vision. Invest Ophthalmol Vis Sci. 2008; 49:3812–3820. [PubMed: 18502992]

Crouch RK, Hazard ES, Lind T, Wiggert B, Chader G, Corson DW. Interphotoreceptor retinoid-binding protein and alpha-tocopherol preserve the isomeric and oxidation state of retinol. Photochem Photobiol. 1992; 56:251–255. [PubMed: 1502268]

Cunningham LL, Gonzalez-Fernandez F. Coordination between production and turnover of interphotoreceptor retinoid-binding protein in zebrafish. Invest OphthalmolVisSci. 2000; 41:3590–3599.

den Hollander AI, McGee TL, Ziviello C, Banfi S, Dryja TP, Gonzalez-Fernandez F, Ghosh D, Berson EL. A homozygous missense mutation in the IRBP gene (RBP3) associated with autosomal recessive retinitis pigmentosa. Invest Ophthalmol Vis Sci. 2009; 50:1864–1872. [PubMed: 19074801]

DesJardin LE, Timmers AM, Hauswirth WW. Transcription of photoreceptor genes during fetal retinal development. Evidence for positive and negative regulation. J Biol Chem. 1993; 268:6953–6960. [PubMed: 8463227]

Dettai A, Lecointre G. New insights into the organization and evolution of vertebrate IRBP genes and utility of IRBP gene sequences for the phylogenetic study of the Acanthomorpha (Actinopterygii: Teleostei). Molecular Phylogenetics and Evolution. 2008; 48:258–269. [PubMed: 18499481]

Do CB, Mahabhashyam MS, Brudno M, Batzoglou S. ProbCons: Probabilistic consistency-based multiple sequence alignment. Genome Res. 2005; 15:330–340. [PubMed: 15687296]

Duffy M, Sun Y, Wiggert B, Duncan T, Chader GJ, Ripps H. Interphotoreceptor retinoid binding protein (IRBP) enhances rhodopsin regeneration in the experimentally detached retina. Experimental Eye Research. 1993; 57:771–782. [PubMed: 8150029]

Edwards RB, Adler AJ. IRBP enhances removal of 11- cis -retinaldehyde from isolated RPE membranes. Experimental Eye Research. 2000; 70:235–245. [PubMed: 10655150]

Fechteler T, Dengler U, Schomburg D. Prediction of protein three-dimensional structures in insertion and deletion regions: a procedure for searching data bases of representative protein fragments using geometric scoring criteria. J Mol Biol. 1995; 253:114–131. [PubMed: 7473707]

Flannery JG, O'Day W, Pfeffer BA, Horwitz J, Bok D. Uptake, processing and release of retinoids by cultured human retinal pigment epithelium. Experimental Eye Research. 1990; 51:717–728. [PubMed: 2265683]

Fleisch VC, Neuhauss SC. Parallel visual cycles in the zebrafish retina. Prog Retin Eye Res. 2010; 29:476–486. [PubMed: 20488254]

Fleisch VC, Schonthaler HB, von Lintig J, Neuhauss SC. Subfunctionalization of a retinoid-binding protein provides evidence for two parallel visual cycles in the cone-dominant zebrafish retina. J Neurosci. 2008; 28:8208–8216. [PubMed: 18701683]

Gonzalez-Fernandez F. Interphotoreceptor retinoid-binding protein--an old gene for new eyes. Vision Research. 2003; 43:3021–3036. [PubMed: 14611938]

Gonzalez-Fernandez F. Interphotoreceptor retinoid binding protein; myths and mysteries. Journal of Ophthalmic & Vision Research. 2012; 7:100–104. [PubMed: 22737397]

Gonzalez-Fernandez F, Baer CA, Baker E, Okajima TI, Wiggert B, Braiman MS, Pepperberg DR. Fourth module of Xenopus interphotoreceptor retinoid-binding protein: activity in retinoid transfer between the retinal pigment epithelium and rod photoreceptors. Current Eye Research. 1998; 17:1150–1157. [PubMed: 9872537]

Gonzalez-Fernandez F, Baer CA, Ghosh D. Module structure of interphotoreceptor retinoid-binding protein (IRBP) may provide bases for its complex role in the visual cycle - structure / function study of Xenopus IRBP. BMC Biochem. 2007; 8:15. [PubMed: 17683573]

Gonzalez-Fernandez F, Betts-Obregon B, Yust B, Mimun J, Sung D, Sardar D, Tsin AT. Interphotoreceptor Retinoid-Binding Protein Protects Retinoids from Photodegradation. Photochem Photobiol. 2015

Gonzalez-Fernandez F, Bevilacqua T, Lee KI, Chandrashekar R, Hsu L, Garlipp MA, Griswold JB, Crouch RK, Ghosh D. Retinol-binding site in interphotoreceptor retinoid-binding protein (IRBP): a novel hydrophobic cavity. Invest Ophthalmol Vis Sci. 2009; 50:5577–5586. [PubMed: 19608538]

Gonzalez-Fernandez F, Ghosh D. Focus on Molecules: interphotoreceptor retinoid-binding protein (IRBP). Experimental Eye Research. 2008; 86:169–170. [PubMed: 17222825]

Gonzalez-Fernandez F, Healy JI. Early expression of the gene for interphotoreceptor retinol-binding protein during photoreceptor differentiation suggests a critical role for the interphotoreceptor matrix in retinal development. J Cell Biol. 1990; 111:2775–2784. [PubMed: 1703544]

Gonzalez-Fernandez F, Sung D, Haswell KM, Tsin A, Ghosh D. Thiol-dependent antioxidant activity of interphotoreceptor retinoid-binding protein. Exp Eye Res. 2014

Gonzalez-Fernandez F, Van Niel E, Edmonds C, Beaver H, Nickerson JM, Garcia-Fernandez JM, Campohiaro PA, Foster RG. Differential expression of interphotoreceptor retinoid-binding protein, opsin, cellular retinaldehyde-binding protein, and basic fibroblastic growth factor. Exp Eye Res. 1993; 56:411–427. [PubMed: 7916695]

Gross EA, Li GR, Lin ZY, Ruuska SE, Boatright JH, Mian IS, Nickerson JM. Prediction of structural and functional relationships of Repeat 1 of human interphotoreceptor retinoid-binding protein (IRBP) with other proteins. Mol Vis. 2000; 6:30–39. [PubMed: 10756179]

Haun RS, Serventi IM, Moss J. Rapid, reliable ligation-independent cloning of PCR products using modified plasmid vectors. Biotechniques. 1992; 13:515–518. [PubMed: 1362067]

Hauswirth WW, Langerijt AV, Timmers AM, Adamus G, Ulshafer RJ. Early expression and localization of rhodopsin and interphotoreceptor retinoid-binding protein (IRBP) in the developing fetal bovine retina. Exp Eye Res. 1992; 54:661–670. [PubMed: 1623951]

Hessler RB, Baer CA, Bukelman A, Kittredge KL, Gonzalez-Fernandez F. Interphotoreceptor retinoid-binding protein (IRBP): expression in the adult and developing Xenopus retina. J Comp Neurol. 1996; 367:329–341. [PubMed: 8698895]

Jin M, Li S, Nusinowitz S, Lloyd M, Hu J, Radu RA, Bok D, Travis GH. The role of interphotoreceptor retinoid-binding protein on the translocation of visual retinoids and function of cone photoreceptors. Journal of Neuroscience. 2009; 29:1486–1495. [PubMed: 19193895]

Lamb TD, Pugh EN Jr. Dark adaptation and the retinoid cycle of vision. Progress in Retinal and Eye Research. 2004; 23:307–380. [PubMed: 15177205]

Lamb TD, Pugh EN Jr. Phototransduction, dark adaptation, and rhodopsin regeneration the proctor lecture. Investigative Ophthalmology and Visual Science. 2006; 47:5137–5152. [PubMed: 17122096]

Levitt M. Accurate modeling of protein conformation by automatic segment matching. J Mol Biol. 1992; 226:507–533. [PubMed: 1640463]

Li L, Nakaya N, Chavali VR, Ma Z, Jiao X, Sieving PA, Riazuddin S, Tomarev SI, Ayyagari R, Riazuddin SA, Hejtmancik JF. A mutation in ZNF513, a putative regulator of photoreceptor development, causes autosomal-recessive retinitis pigmentosa. Am J Hum Genet. 2010; 87:400–409. [PubMed: 20797688]

Li S, Yang Z, Hu J, Gordon WC, Bazan NG, Haas AL, Bok D, Jin M. Secretory defect and cytotoxicity: the potential disease mechanisms for the retinitis pigmentosa (RP)-associated interphotoreceptor retinoid-binding protein (IRBP). J Biol Chem. 2013; 288:11395–11406. [PubMed: 23486466]

Li WH, Zhou L, Li Z, Wang Y, Shi JT, Yang YJ, Gui JF. Zebrafish Lbh-like Is Required for Otx2-mediated Photoreceptor Differentiation. Int J Biol Sci. 2015; 11:688–700. [PubMed: 25999792]

Lin ZY, Li GR, Takizawa N, Si JS, Gross EA, Richardson K, Nickerson JM. Structure-function relationships in interphotoreceptor retinoid-binding protein (IRBP). Mol Vis. 1997; 3:17. [PubMed: 9479008]

Liou GI, Geng L, Baehr W. Interphotoreceptor retinoid-binding protein: biochemistry and molecular biology. Progress in Clinical and Biological Research. 1991; 362:115–137. [PubMed: 2003123]

Loew A, Baer C, Gonzalez-Fernandez F. The functional unit of interphotoreceptor retinoid-binding protein (IRBP)--purification, characterization and preliminary crystallographic analysis. Exp Eye Res. 2001; 73:257–264. [PubMed: 11446776]

Loew A, Gonzalez-Fernandez F. Crystal structure of the functional unit of interphotoreceptor retinoid binding protein. Structure. 2002a; 10:43–49. [PubMed: 11796109]

Loew A, Gonzalez-Fernandez F. Crystal structure of the functional unit of interphotoreceptor retinoid binding protein. Structure. 2002b; 10:43–49. [PubMed: 11796109]

Marmor MF, Martin LJ. 100 years of the visual cycle. Survey of Ophthalmology. 1978; 22:279–285. [PubMed: 345511]

Mata NL, Radu RA, Clemmons RC, Travis GH. Isomerization and oxidation of vitamin a in cone-dominant retinas: a novel pathway for visual-pigment regeneration in daylight. Neuron. 2002; 36:69–80. [PubMed: 12367507]

Mata NL, Ruiz A, Radu RA, Bui TV, Travis GH. Chicken retinas contain a retinoid isomerase activity that catalyzes the direct conversion of all-trans-retinol to 11-cis-retinol. Biochemistry. 2005; 44:11715–11721. [PubMed: 16128572]

McBee JK, Palczewski K, Baehr W, Pepperberg DR. Confronting complexity: the interlink of phototransduction and retinoid metabolism in the vertebrate retina. Progress in Retinal and Eye Research. 2001; 20:469–529. [PubMed: 11390257]

Monod J, Wyman J, Changeux JP. On the nature of allosteric transitions: a plausible model. J Mol Biol. 1965; 12:88–118. [PubMed: 14343300]

Muniz A, Villazana-Espinoza ET, Hatch AL, Trevino SG, Allen DM, Tsin AT. A novel cone visual cycle in the cone-dominated retina. Experimental Eye Research. 2007; 85:175–184. [PubMed: 17618621]

Murshudov GN, Vagin AA, Dodson EJ. Refinement of macromolecular structures by the maximum-likelihood method. Acta Crystallogr D Biol Crystallogr. 1997; 53:240–255. [PubMed: 15299926]

Nickerson JM, Borst DE, Redmond TM, Si JS, Toffenetti J, Chader GJ. The molecular biology of IRBP: application to problems of uveitis, protein chemistry, and evolution. Progress in Clinical and Biological Research. 1991; 362:139–161. [PubMed: 2003124]

Nickerson JM, Frey RA, Ciavatta VT, Stenkamp DL. Interphotoreceptor retinoid-binding protein gene structure in tetrapods and teleost fish. Mol Vis. 2006; 12:1565–1585. [PubMed: 17200656]

Nickerson JM, Li GR, Lin ZY, Takizawa N, Si JS, Gross EA. Structure-function relationships in the four repeats of human interphotoreceptor retinoid-binding protein (IRBP). Mol Vis. 1998; 4:33. [PubMed: 9873071]

Okajima TI, Pepperberg DR, Ripps H, Wiggert B, Chader GJ. Interphotoreceptor retinoid-binding protein: role in delivery of retinol to the pigment epithelium. Experimental Eye Research. 1989; 49:629–644. [PubMed: 2509230]

Okajima TI, Pepperberg DR, Ripps H, Wiggert B, Chader GJ. Interphotoreceptor retinoid-binding protein promotes rhodopsin regeneration in toad photoreceptors. Proceedings of the National Academy of Sciences of the United States of America. 1990; 87:6907–6911. [PubMed: 2118660]

Owens, RJ.; Nettleship, JE.; Berrow, NS.; Sainsbury, S.; Radu, RA.; Stuart, DI.; Stammers, DK. High-throughput cloning, expression, and purification. In: Sanderson, MR.; Skelly, JV., editors. Macromolecular Crystallography: Conventional and High-Throughput Methods. Oxford University Press; Oxford: 2007. p. 23-44.

Page MJ, Di Cera E. Serine peptidases: classification, structure and function. Cell Mol Life Sci. 2008; 65:1220–1236. [PubMed: 18259688]

Parker R, Wang JS, Kefalov VJ, Crouch RK. Interphotoreceptor Retinoid-Binding Protein as the Physiologically Relevant Carrier of 11-cis-Retinol in the Cone Visual Cycle. J Neurosci. 2011; 31:4714–4719. [PubMed: 21430170]

Pepperberg DR, Okajima TL, Wiggert B, Ripps H, Crouch RK, Chader GJ. Interphotoreceptor retinoid-binding protein (IRBP). Molecular biology and physiological role in the visual cycle of rhodopsin. Molecular Neurobiology. 1993; 7:61–85. [PubMed: 8318167]

Putilina T, Sittenfeld D, Chader GJ, Wiggert B. Study of a fatty acid binding site of interphotoreceptor retinoid-binding protein using fluorescent fatty acids. Biochemistry. 1993; 32:3797–3803. [PubMed: 8466918]

Qtaishat NM, Wiggert B, Pepperberg DR. Interphotoreceptor retinoid-binding protein (IRBP) promotes the release of all-trans retinol from the isolated retina following rhodopsin bleaching illumination. Experimental Eye Research. 2005; 81:455–463. [PubMed: 15935345]

Rajendran RR, Van Niel EE, Stenkamp DL, Cunningham LL, Raymond PA, Gonzalez-Fernandez F. Zebrafish interphotoreceptor retinoid-binding protein: differential circadian expression among cone subtypes. J Exp Biol. 1996; 199:2775–2787. [PubMed: 9110959]

Rawlings ND, Barrett AJ, Bateman A. MEROPS: the database of proteolytic enzymes, their substrates and inhibitors. Nucleic Acids Res. 2012; 40:D343–350. [PubMed: 22086950]

Rhodes, G. Crystallography Made Crystal Clear. Academic Press; 2006.

Schonthaler HB, Lampert JM, Isken A, Rinner O, Mader A, Gesemann M, Oberhauser V, Golczak M, Biehlmaier O, Palczewski K, Neuhauss SC, von Lintig J. Evidence for RPE65-independent vision

in the cone-dominated zebrafish retina. Eur J Neurosci. 2007; 26:1940–1949. [PubMed: 17868371]

Semenova EM, Converse CA. Comparison between oleic acid and docosahexaenoic acid binding to interphotoreceptor retinoid-binding protein. Vision Res. 2003; 43:3063–3067. [PubMed: 14611942]

Sparrow JR, Fishkin N, Zhou J, Cai B, Jang YP, Krane S, Itagaki Y, Nakanishi K. A2E, a byproduct of the visual cycle. Vision Res. 2003; 43:2983–2990. [PubMed: 14611934]

Stenkamp DL, Cunningham LL, Raymond PA, Gonzalez-Fernandez F. Novel expression pattern of interphotoreceptor retinoid-binding protein (IRBP) in the adult and developing zebrafish retina and RPE. Mol Vis. 1998; 4:26. [PubMed: 9841935]

Szuts EZ, Harosi FI. Solubility of retinoids in water. Arch Biochem Biophys. 1991; 287:297–304. [PubMed: 1898007]

Takahashi Y, Moiseyev G, Chen Y, Nikolaeva O, Ma JX. An alternative isomerohydrolase in the retinal Muller cells of a cone-dominant species. FEBS J. 2011; 278:2913–2926. [PubMed: 21676174]

Thompson DA, Gal A. Vitamin A metabolism in the retinal pigment epithelium: genes, mutations, and diseases. Progress in Retinal and Eye Research. 2003; 22:683–703. [PubMed: 12892646]

Trevino SG, Villazana-Espinoza ET, Muniz A, Tsin AT. Retinoid cycles in the cone-dominated chicken retina. Journal of Experimental Biology. 2005; 208:4151–4157. [PubMed: 16244173]

Tsina E, Chen C, Koutalos Y, Ala-Laurila P, Tsacopoulos M, Wiggert B, Crouch RK, Cornwall MC. Physiological and microfluorometric studies of reduction and clearance of retinal in bleached rod photoreceptors. Journal of General Physiology. 2004a; 124:429–443. [PubMed: 15452202]

Tsina E, Chen C, Koutalos Y, Ala-Laurila P, Tsacopoulos M, Wiggert B, Crouch RK, Cornwall MC. Physiological and microfluorometric studies of reduction and clearance of retinal in bleached rod photoreceptors. J Gen Physiol. 2004b; 124:429–443. [PubMed: 15452202]

Wang JS, Kefalov VJ. The cone-specific visual cycle. Prog Retin Eye Res. 2011; 30:115–128. [PubMed: 21111842]

Ward, LD. Measurement of ligand binding to protein by fluorescence spectroscopy. In: Hirs, CHW.; Timasheff, SN., editors. Methods Enzymol. Academic press; New York: 1985. p. 400-414.

Winn MD, Ballard CC, Cowtan KD, Dodson EJ, Emsley P, Evans PR, Keegan RM, Krissinel EB, Leslie AG, McCoy A, McNicholas SJ, Murshudov GN, Pannu NS, Potterton EA, Powell HR, Read RJ, Vagin A, Wilson KS. Overview of the CCP4 suite and current developments. Acta Crystallogr D Biol Crystallogr. 2011; 67:235–242. [PubMed: 21460441]

Wisard J, Faulkner A, Chrenek MA, Waxweiler T, Waxweiler W, Donmoyer C, Liou GI, Craft CM, Schmid GF, Boatright JH, Pardue MT, Nickerson JM. Exaggerated eye growth in IRBP-deficient mice in early development. Invest Ophthalmol Vis Sci. 2011; 52:5804–5811. [PubMed: 21642628]

Wolf G. Transport of retinoids by the interphotoreceptor retinoid-binding protein. Nutr Rev. 1998; 56:156–158. [PubMed: 9624888]

Wolf G. The visual cycle of the cone photoreceptors of the retina. Nutrition Reviews. 2004; 62:283–286. [PubMed: 15384919]

Wu Q, Blakeley LR, Cornwall MC, Crouch RK, Wiggert BN, Koutalos Y. Interphotoreceptor Retinoid-Binding Protein Is the Physiologically Relevant Carrier That Removes Retinol from Rod Photoreceptor Outer Segments. Biochemistry. 2007; 46:8669–8679. [PubMed: 17602665]

Highlights

- Fatty acids have been proposed to regulate retinoid trafficking by IRBP
- However, nothing is known about the structure of IRBP-fatty acid interactions
- We determined the X-ray crystal structure of the zebrafish IRBP module one (z1)
- Z1 consists of domains A & B with a novel oleic acid binding pocket in domain B
- The holoIRBP structure is consistent with fatty acids regulating retinoid trafficking

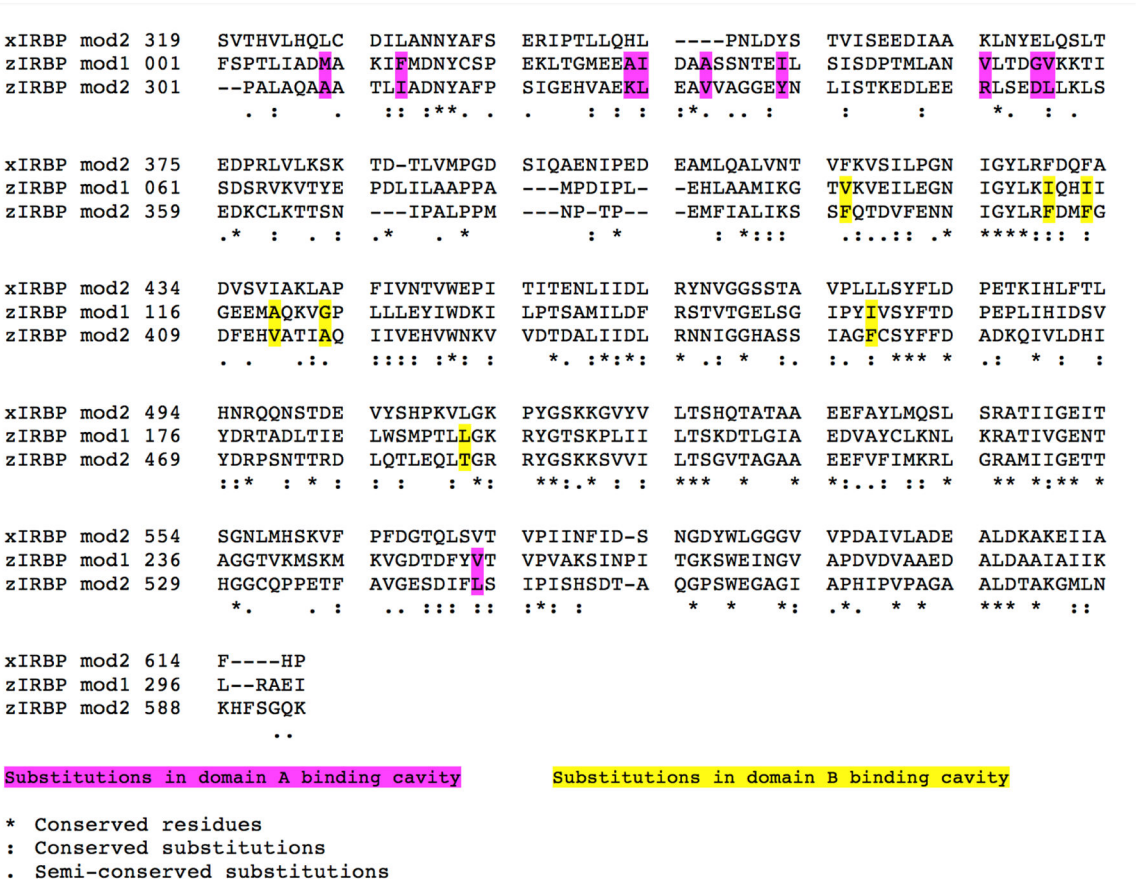

Figure 1. Alignment of the amino acid sequences of modules of IRBPs: *Xenopus* module 2 (xIRBP mod2), zebrafish (zIRBP) module 1 (mod1) and module 2 (mod2)

Functionally important substitutions are highlighted and color-coded.

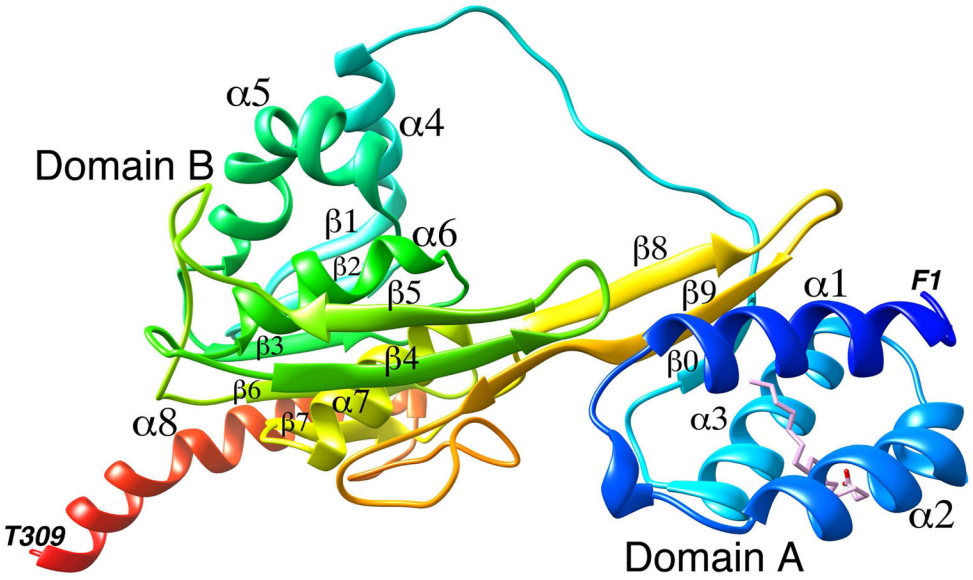

Figure 2. A ribbon diagram of the crystal structure of zebrafish IRBP module 1

The N terminus is shown in blue and the C terminus in red. The domains and the secondary structure elements are marked. The oleic acid (OLA) binding site is shown with the bound oleic acid molecule. The terminal amino acids are also marked.

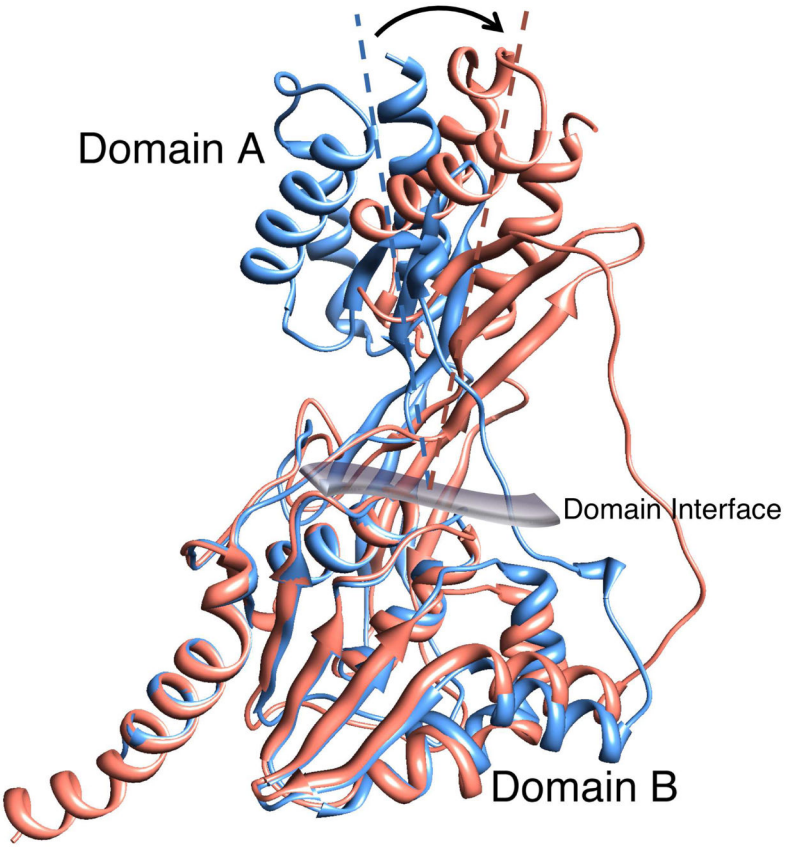

Figure 3. Superposition of the crystal structures of zebrafish IRBP module 1 (salmon) and *Xenopus* IRBP module 2 (blue)

The N-terminal domain A's appear to be rotated roughly 21±4° from each other (resembling the rotation of the imaginary A-domain axis as shown) about the viewing axis of the figure at the domain interface.

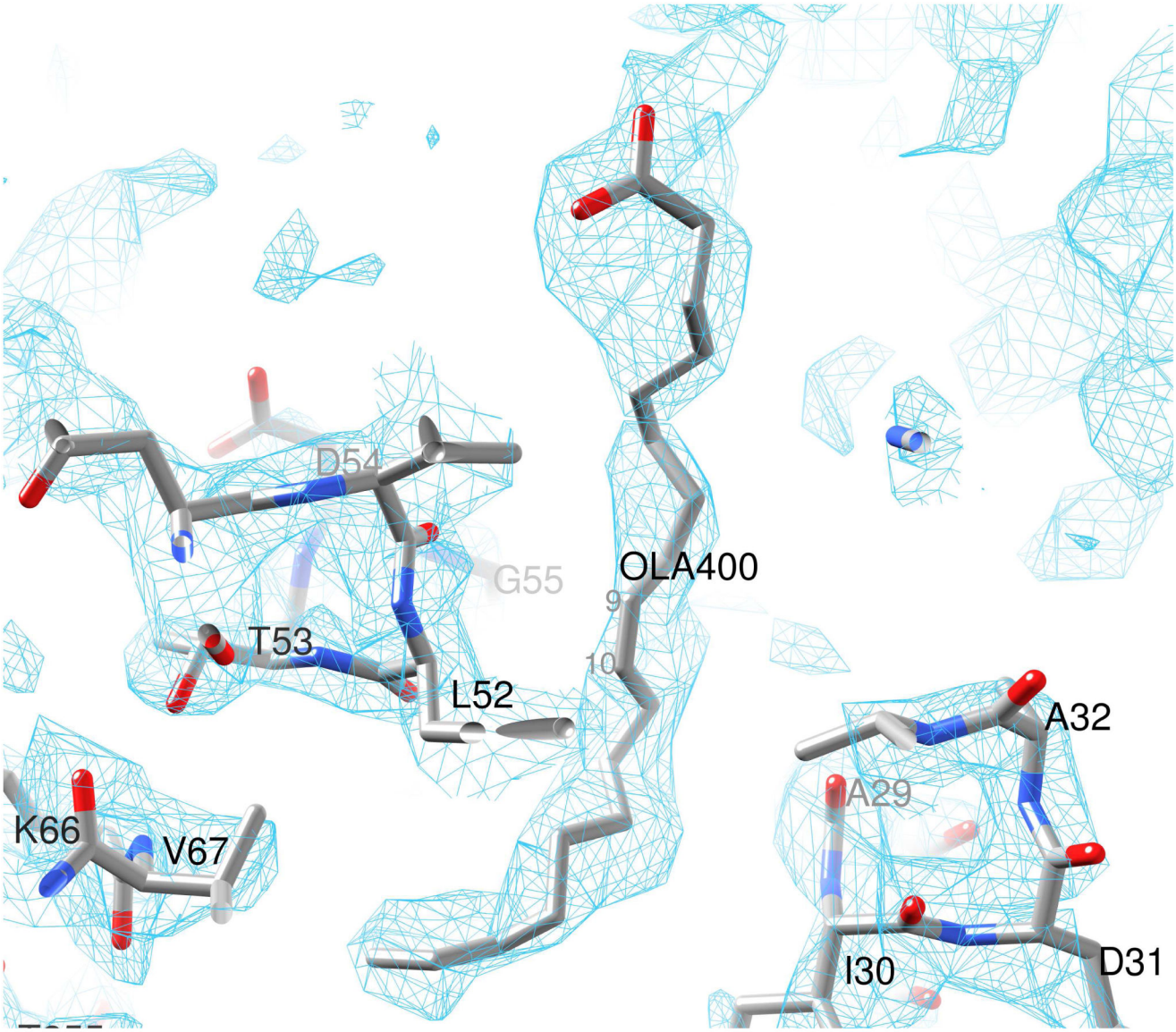

Figure 4. Electron density ($2F_{obs}-F_{cal}$) omit map for the bound oleic acid (OLA) molecule in domain A

The electron density map is contoured at 1σ. Atoms C9 and C10 are labeled to indicate the location of the C9=C10 *cis* double bond.

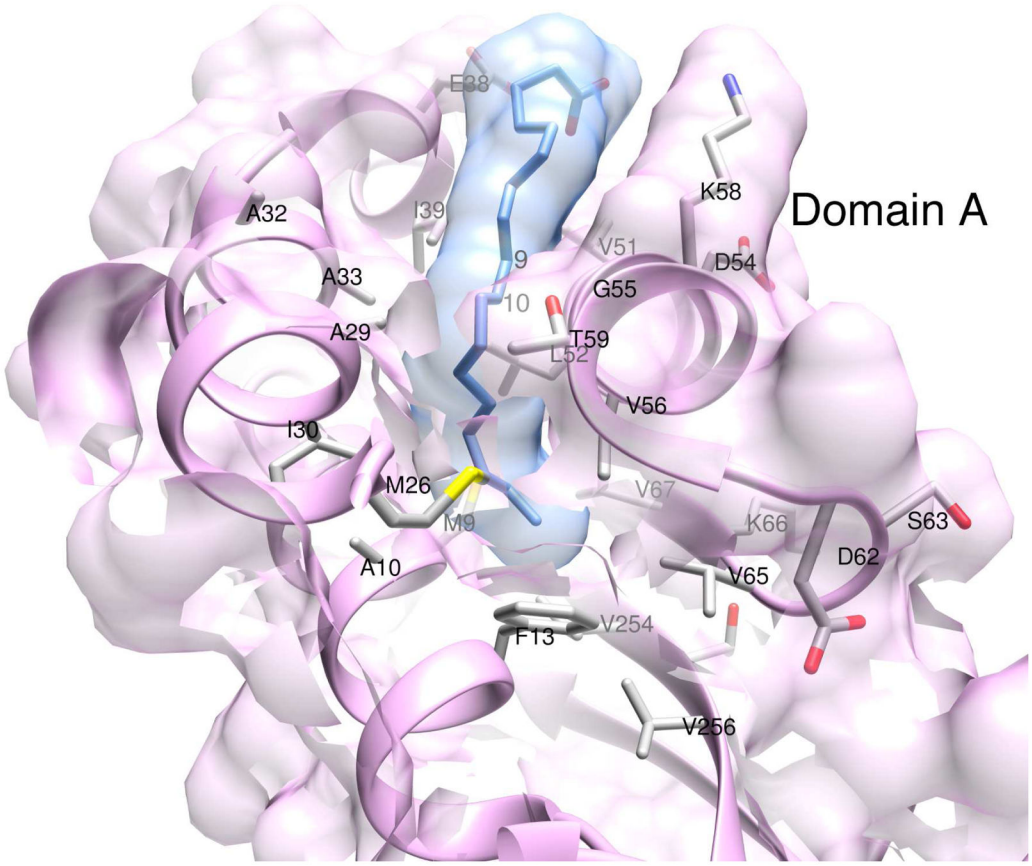

Figure 5. Oleic acid binding site in domain A of zIRBP module 1

Important amino acid side chains inside the cavities and at the perimeter are shown. van der Waals surfaces of ligand and protein atoms are depicted in semi-transparent colors. The location of the C9=C10 *cis* double bond is marked by the labels 9 and 10.

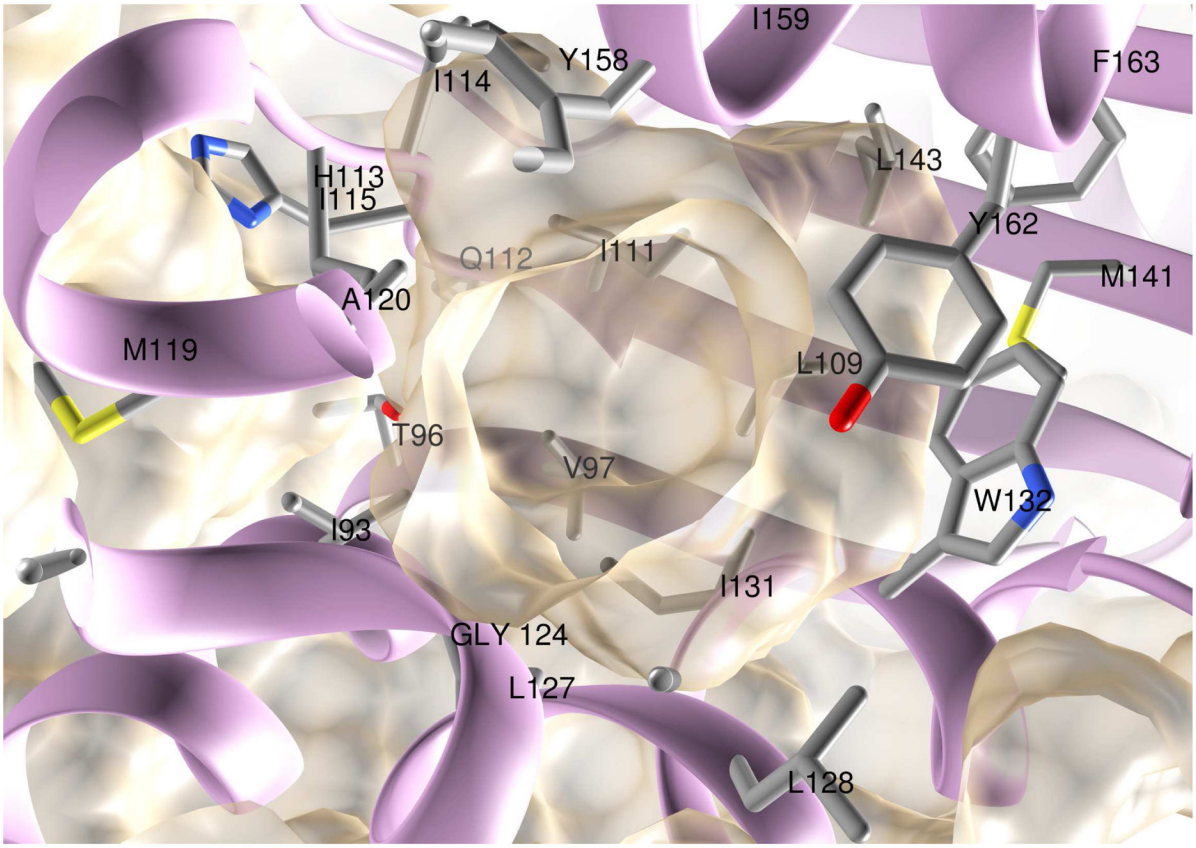

Figure 6. Hydrophobic cavity in domain B

The semi-transparent van der Waals surface of the protein atoms is shown along with the protein backbone. Side chains that line the cavity are also shown.

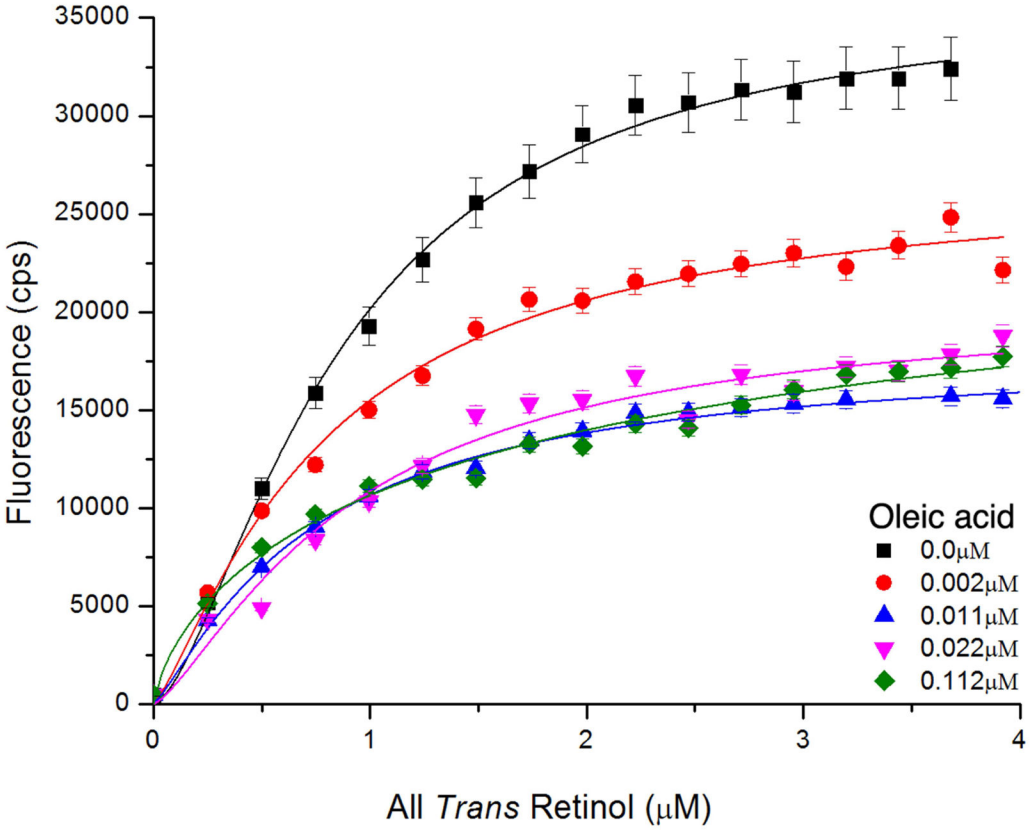

Figure 7. Fluorescent spectroscopic titration of all-*trans* retinol binding to zIRBP (1μM)
Monitoring enhancement of all-*trans* retinol fluorescence in the presence of 0.0μM (■), 0.0022μM (●), 0.0112μM ▲), 0.02225μM (▼), 0.112μM (◆) of oleic acid.

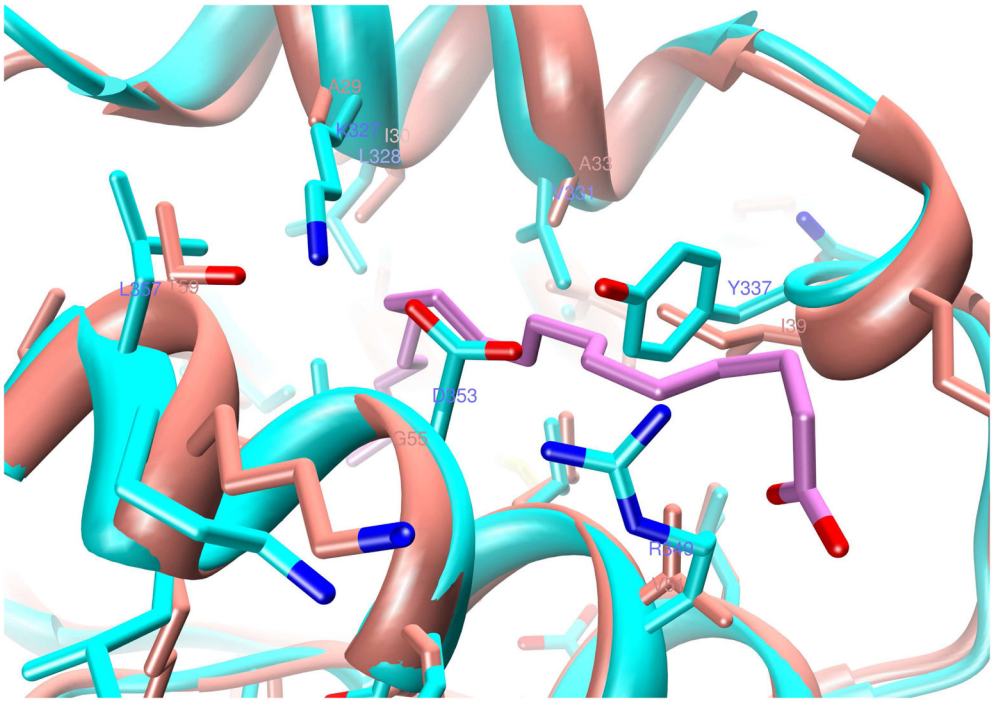

Figure 8. Homology modeling of module 2 (z2, in cyan) after z1 (in salmon color)

Several small-to-large side chain substitutions at the cavity perimeter as well as within the interior in domain A are depicted. The location of oleic acid C9=C10 *cis* double bond is marked by the labels 9 and 10. But for some structural rearrangements, these substitutions are therefore likely to eliminate this oleic acid binding site from z2.

Table 1

Summary of X-ray diffraction data collection and structure refinement

Table 1A. Data collection summary at the absorption edge of Se							
Wavelength (Å)	**Total data**	**Unique data**	**Resolution (Å)**	**% Completion (Outer shell)**	**R_{merge} Overall (outer shell)**	**Overall I/σI**	**Outer shell I/σI**
Peak 0.9793680	181,866	27,170	1.90	99.6 (99.8)	0.095 (0.64)	38.5	2.8
Remote 0.9716932	184,724	27,277	1.90	99.8 (99.9)	0.085 (0.60)	40.0	2.0
Inflection 0.9794840	104,752	15,863	2.30	97.5 (98.5)	0.082 (0.56)	39.4	1.7

Table 1B. Refinement summary	
Crystal parameters[*]:	
Space group	$P2_12_12$
Unit cell parameters	
a, *b*, *c* (Å)	83.295, 97.771, 41.214
α, *β*, *γ* (°)	90.0, 90.0, 90.0
Resolution (Å)	1.90 (1.901–1.950)[*]
Refinement:	
Resolution range (Å)	63.32 – 1.90
No. reflections (structure amplitude *F>0*)	25,467
Completeness (%)	98.3 (95.0)
R_{work} / R_{free}	0.219/0.268
Number of atoms	2556
Protein	2338
Ligands (HEPES, glycerol, oleic acid)	53
Water	165
Wilson plot *B-factor* (Å^2)	29.7
B-factors (Å^2) all atoms	33.4
Protein	32.4
Water	41.3
HEPES, glycerol	42.2
Oleic acid	70.2

Table 1B. Refinement summary	
R.m.s. deviations	
Bond lengths (Å)	0.012
Bond angles (°)	1.374
* Values in parentheses are for highest-resolution shell.	
Ramachandran plot statistics	
In preferred regions	97.7%

* Bernhard Rupp, Biomolecular Crystallography Principles, Practice, and Application to Structural Biology (2010), Garland Science, Taylor and Francis Group, New York, NY, USA.

Table 2

Binding titration of all-*trans* retinol to zebrafish IRBP in the absence/presence of oleic acid

Oleic acid concentration (μM)	K_d ± S.E. (μM)	Hill Coefficient ± S.E.
0.000	0.91 ± 0.05	1.84 ± 0.24
0.002	0.90 ± 0.14	1.79 ± 0.57
0.011	0.83 ± 0.12	1.47 ± 0.35
0.022	0.95 ± 0.13	1.97 ± 0.59
0.112	1.82 ± 1.49	0.83 ± 0.66